ISSN 1070-3284, Russian Journal of Coordination Chemistry, 2017, Vol. 43, No. 5, pp. 286–296. © Pleiades Publishing, Ltd., 2017.
Original Russian Text © O.V. Loseva, T.A. Rodina, A.V. Gerasimenko, A.V. Ivanov, 2017, published in Koordinatsionnaya Khimiya, 2017, Vol. 43, No. 5, pp. 290–300.

Principles of Supramolecular Polymeric Chain Formation in Heteronuclear Gold(III)–Iron(III) Complexes ($[Au(S_2CNR_2)_2][FeCl_4]$)$_n$ (R = C_3H_7, *iso*-C_3H_7): Chemisorption Synthesis, Structural Organization, and Thermal Behavior

O. V. Loseva[a], T. A. Rodina[b], A. V. Gerasimenko[c], and A. V. Ivanov[a, *]

[a] *Institute of Geology and Nature Management, Far East Branch, Russian Academy of Sciences, Blagoveshchensk, Russia*

[b] *Amur State University, Blagoveshchensk, Russia*

[c] *Institute of Chemistry, Far East Branch, Russian Academy of Sciences, Vladivostok, Russia*

**e-mail: alexander.v.ivanov@chemist.com*

Received July 4, 2016

Abstract—Polymeric gold(III)–iron(III) dithiocarbamate–chloride complexes of the ionic type are synthesized by the chemisorption binding of gold(III) with freshly precipitated iron(III) dipropyl and di-*iso*-propyl dithiocarbamates from solutions of $H[AuCl_4]$ in 2 M HCl. Heteropolynuclear complexes of the compositions ($[Au\{S_2CN(C_3H_7)_2\}_2][FeCl_4]$)$_n$ (**I**) and ($[Au\{S_2CN(iso\text{-}C_3H_7)_2\}_2][FeCl_4]$)$_n$ (**II**) are preparatively isolated as individual forms of gold(III) binding. The structural organization of the complexes is established by X-ray diffraction analysis (CIF files CCDC no. 1480802 (**I**) and no. 1480806 (**II**)). The structures of compounds **I** and **II** are characterized at the supramolecular level by the presence of two types of polymeric chains, the methods of formation of which differ substantially. Compound **I** contains the following structural units: four structurally nonequivalent centrosymmetric complex cations $[Au\{S_2CN(C_3H_7)_2\}_2]^+$ (A, B, C, and D) and two complex anions $[FeCl_4]^-$ related to each other as conformers. Two independent cation-cationic linear polymeric chains (···A···B···)$_n$ and (···C···D···)$_n$ are formed in the structure of complex **I** due to pair relatively weak secondary interactions Au···S (nonvalent type) between the adjacent complex cations. The structure of compound **II** is characterized by zigzag cation-anionic chains (···$[Au\{S_2CN(iso\text{-}C_3H_7)_2\}_2]^+$···$[FeCl_4]^-$···)$_n$ in the formation of which the secondary interactions Au···Cl play the determining role. The thermal behavior of complexes **I** and **II** is studied by simultaneous thermal analysis. The thermal destruction process includes the thermolysis of the dithiocarbamate moiety of the complexes and $[FeCl_4]^-$ with the reduction of gold(III) to the metal, the liberation of $FeCl_3$, and the partial transformation of the latter into Fe_2O_3. In both cases, the final products of the thermal transformations of the studied compounds are elemental gold and Fe_2O_3.

Keywords: heteronuclear gold(III)–iron(III) dithiocarbamate–chloride complexes, chemisorption synthesis, supramolecular structures, structural self-organization, secondary bonds, thermal behavior

DOI: 10.1134/S1070328417050049

INTRODUCTION

Interest in studying coordination compounds of iron(III) with dithiocarbamate ligands (using IR, EPR, and heteronuclear ^1H, ^{13}C, and ^{15}N NMR spectroscopy) is due to their anomalous magnetic and electronic properties (for example, [1–5]). Iron(III) dithiocarbamates are used as initiators of polymerization for the preparation of polystyrene and polymethylmethacrylate [6] and as selective traps for the detection and quantitative determination of nitrogen monoxide (NO) in cells and tissues of plants and animals [7–9]. In addition, the capability of efficient chemisorption binding of gold(III) from solutions was established for dithiocarbamates of a series of transition and post-transition metals. As a result, numerous polymeric heteronuclear complexes containing cadmium and zinc along with gold(III) were preparatively isolated and characterized in detail: ($[Au(S_2CNR_2)_2]_2X$)$_n$ (X = $[CdCl_4]^{2-}$, $[Cd_2Cl_6]^{2-}$, $[ZnCl_4]^{2-}$) [10–12], ($[H_3O][Au_3(S_2CNR_2)_6]$-$[ZnCl_4]_2$)$_n$ [13, 14]), and ($[NH_2R_2][Au(S_2CNR_2)_2]X$)$_n$ (X = $[CdCl_4]^{2-}$, $[ZnCl_4]^{2-}$) [15, 16]); as well as compounds containing bismuth ($[Au(S_2CNR_2)_2]_3X$)$_n$ (X = $[Bi_2Cl_9]^{3-}$, $[Bi_3Cl_{12}]^{3-}$) [17, 18], thallium(III) ($[Au(S_2CNR_2)_2][TlCl_4]$)$_n$ [19, 20], and iron(III) ($[Au(S_2CNR_2)_2][FeCl_4]$)$_n$ (R = C_4H_9, *iso*-C_4H_9) [21]

together with gold(III). Diverse complicatedly organized supramolecular structures are formed for the obtained compounds due to secondary (Au···S, Au···Cl, S···Cl) and aurophilic (Au···Au) interactions of various types.

Continuing these investigations, the chemisorption binding of gold(III) with freshly precipitated iron(III) dialkyl dithiocarbamates of the general composition $[Fe(S_2CNR_2)_3]$ (R = C_3H_7, *iso*-C_3H_7) from solutions of $AuCl_3$ in 2 M HCl was studied in this work. The following new heteropolynuclear gold(III)–iron(III) dithiocarbamate chloride complexes were obtained as individual forms of gold(III) binding: $([Au\{S_2CN(C_3H_7)_2\}_2][FeCl_4])_n$ (**I**) and $([Au\{S_2CN(iso\text{-}C_3H_7)_2\}_2][FeCl_4])_n$ (**II**). The crystal structures of compounds **I** and **II** established by X-ray diffraction analysis are characterized by the formation of supramolecular cation-cationic (**I**) and cation-anionic (**II**) polymeric chains due to the participation of secondary interactions Au···S (**I**) and Au···Cl (**II**) of the nonvalent type. The thermal behavior of compounds **I** and **II** was studied by simultaneous thermal analysis (STA).

EXPERIMENTAL

Sodium dipropyl and di-*iso*-propyl dithiocarbamates were obtained by the reactions of carbon bisulfide (Merck) with dipropylamine (Merck) or di-*iso*-propylamine (Sigma) in an alkaline medium. The starting iron(III) complexes were prepared by the precipitation of Fe^{3+} ions from the aqueous phase with the corresponding sodium dithiocarbamates taken in stoichiometric amounts [22]. The individual character of the obtained crystalline sodium salts was established by the ^{13}C MAS NMR method, δ, ppm:

$Na\{S_2CN(C_3H_7)_2\} \cdot H_2O$ (1 : 2 : 2 : 2): 208.3 ($-S_2CN=$); 59.4, 57.9 (1 : 1, $=NCH_2-$); 22.3, 21.5 (1 : 1, $-CH_2-$); 12.6, 11.5 (1 : 1, $-CH_3$).

$Na\{S_2CN(iso\text{-}C_3H_7)_2\} \cdot 3H_2O$ (1 : 2 : 4): 206.6 ($-S_2CN=$); 58.6, 51.3 (1 : 1, =NCH=); 21.7, 19.8 (3 : 1, $-CH_3$).

Synthesis of compounds I and II. Polymeric bis(*N*,*N*-dipropyldithiocarbamato-*S*,*S*')gold(III) (**I**) and bis(*N*,*N*-di-*iso*-propyldithiocarbamato-*S*,*S*')gold(III) (**II**) tetrachloroferrates(III) were synthesized by the reactions of freshly precipitated iron(III) dithiocarbamates $[Fe(S_2CNR_2)_3]$ (R = C_3H_7, *iso*-C_3H_7) with solutions of $AuCl_3$ in 2 M HCl. A solution (10 mL) of $AuCl_3$ (in 2 M HCl) containing gold (~34 mg) was poured to each black-colored iron(III) complex (100 mg), and the mixture was stirred for 60 min. The residual content of gold and the iron content in the solution were determined on a Hitachi atomic absorption spectrometer (class 1, model 180-50). The obtained yellow-brown precipitates were filtered off, washed with water, and dried on a filter. The prismatic crystals of complexes **I** and **II** for X-ray diffraction analysis were obtained from acetone and an acetone–toluene (1 : 1) mixture, respectively.

X-ray diffraction analysis was carried out for the single crystals of compounds **I** and **II** on BRUKER Kappa APEX2/BRUKER Smart APEX2 diffractometers (MoK_α radiation, λ = 0.71073 Å, graphite monochromator) at 170(2) or 296(2) K. An X-ray absorption correction was applied by equivalent reflections. The structures were determined by a direct method and refined by least squares in the anisotropic approximation of non-hydrogen atoms (for **II**) or in the isotropic approximation of nitrogen and carbon atoms and anisotropic approximation of other non-hydrogen atoms (for **I**). The positions of hydrogen atoms were calculated geometrically and included into refinement by the riding model. In the disordered complex anion $[FeCl_4]^-$ of compound **II**, the site occupancies of the statistically distributed chlorine atoms are specified to be equal to 0.5.

The experimental data were collected and processed and the unit cell parameters were refined using the APEX2 programs [23]. All calculations on structure determination and refinement were performed using the SHELXTL/PC programs [24]. The main crystallographic data and the refinement results for the structures of compounds **I** and **II** are presented in Table 1. Selected bond lengths and angles are given in Table 2.

The coordinates of atoms, bond lengths, and angles were deposited with the Cambridge Crystallographic Data Centre (CIF files no. 1480802 (**I**) and no. 1480806 (**II**); deposit@ccdc.cam.ac.uk or http://www.ccdc.cam.ac.uk).

Thermal behavior of compounds **I** and **II** was studied by the STA method with the simultaneous detection of curves of thermogravimetry (TG) and differential scanning calorimetry (DSC). The studies were carried out on an STA 449C Jupiter instrument (NETZSCH) in corundum crucibles under caps with a hole providing a vapor pressure of 1 atm during the thermal decomposition of the samples at a heating rate of 5°C/min to 1100°C (argon atmosphere). The samples were additionally recorded in aluminum crucibles to reveal heat effects at the initial stage of thermolysis. The weights of the samples were 1.807–6.468 and 2.517–5.571 mg for compounds **I** and **II**, respectively. The accuracy of the temperature measurement was ±0.4°C, and that for the weight change was $\pm 1 \times 10^{-4}$ mg. When recording the TG and DSC curves, a correction file and calibrations for the temperature and sensitivity for

Table 1. Crystallographic data and the experimental and refinement parameters for the structures of compounds **I** and **II**

Parameter	Value	
	Compound **I**	Compound **II**
Empirical formula	$C_{14}H_{28}N_2S_4Cl_4FeAu$	$C_{14}H_{28}N_2S_4Cl_4FeAu$
FW	747.24	747.24
T, K	170(2)	296(2)
Crystal system	Monoclinic	Monoclinic
Space group	$P2_1/c$	$C2/c$
a, Å	30.7684(6)	15.5198(6)
b, Å	8.4605(2)	10.8324(4)
c, Å	21.6874(4)	16.9408(6)
β, deg	110.4290(10)	107.166(1)
V, Å^3	5290.50(19)	2721.2(2)
Z	8	4
ρ_{calcd}, g/cm^3	1.876	1.824
μ, mm^{-1}	6.812	6.622
F(000)	2904	1452
Crystal size, mm	0.04 × 0.05 × 0.32	0.26 × 0.25 × 0.15
Data collection over θ range, deg	1.878–32.064	2.33–28.75
Ranges of reflection indices	$-44 \le h \le 45$, $-12 \le k \le 11$, $-31 \le l \le 32$	$-20 \le h \le 20$, $-14 \le k \le 14$, $-22 \le l \le 22$
Measured reflections	69189	15768
Independent reflections (R_{int})	18425 (0.0395)	3346 (0.0169)
Reflections with $I > 2\sigma(I)$	9008	2897
Refinement variables	483	142
Goodness-of-fit	0.993	1.057
R factors for $F^2 > 2\sigma(F^2)$	$R_1 = 0.0379$, $wR_2 = 0.0710$	$R_1 = 0.0395$, $wR_2 = 0.1117$
R factors for all reflections	$R_1 = 0.1028$, $wR_2 = 0.0891$	$R_1 = 0.0453$, $wR_2 = 0.1163$
Residual electron density (min/max), *e*/Å^3	−0.699/1.422	−1.417/1.230

the specified temperature program and heating rate were used. The independent determination of the melting points of the complexes was carried out on a PTP(M) instrument (OAO Khimlaborpribor).

Electron scanning microscopy and X-ray spectral microanalysis. The dispersion and morphological features of the samples were determined using high resolution electron microscopy on a JSM 6390LV JEOL scanning electron microscope (Japan) equipped with the Oxford INCA Energy 350-Wave microanalysis system (England) with dispersion over energies and wavelengths. The qualitative determination of the chemical composition was carried out by the microprobe method using an energy dispersive spectrometer.

RESULTS AND DISCUSSION

According to the data of electron microscopy, the finely crystalline black precipitates of the starting iron(III) dipropyl and di-*iso*-propyl dithiocarbamates are presented by round particles with a diameter of ~1.3–5.7 μm. In both cases, the shape of the particles and the energy dispersive spectra characterizing the elemental composition of the starting complexes are fairly similar (the data for $[Fe\{S_2CN(C_3H_7)_2\}_3]$ are presented in Figs. 1a and 1a'). The chemisorption binding of gold(III) by iron(III) dithiocarbamates from solutions of $AuCl_3$ in 2 M HCl results in the reformation of the precipitates and a change in their color to yellow-brown. The round particles of the starting complexes are predominantly transformed into prismatic particles enlarged to ~4.8–20.2 μm (Fig. 1b).

Table 2. Selected bond lengths (*d*) and bond (ω) and torsion (φ) angles in the structures of compounds **I** and **II***

Compound **I**			
Cation A		Cation B	
Bond	*d*, Å	Bond	*d*, Å
Au(1)–S(1)	2.3333(10)	Au(2)–S(3)	2.3414(11)
Au(1)–S(2)	2.3288(10)	Au(2)–S(4)	2.3272(10)
Au(1)···S(3)	3.7316(12)	Au(2)···S(1)	3.5316(11)
S(1)–C(1)	1.725(4)	S(3)–C(8)	1.723(4)
S(2)–C(1)	1.730(4)	S(4)–C(8)	1.736(5)
N(1)–C(1)	1.302(5)	N(2)–C(8)	1.300(5)
N(1)–C(2)	1.474(5)	N(2)–C(9)	1.491(6)
N(1)–C(5)	1.472(5)	N(2)–C(12)	1.478(6)
Angle	ω, deg	Angle	ω, deg
S(1)Au(1)S(2)	75.61(3)	S(3)Au(2)S(4)	75.11(4)
S(1)Au(1)S(2)[a]	104.39(3)	S(3)Au(2)S(4)[b]	104.89(4)
C(1)S(1)Au(1)	86.37(13)	C(8)S(3)Au(2)	87.0(2)
C(1)S(2)Au(1)	86.39(13)	C(8)S(4)Au(2)	87.12(14)
S(1)C(1)S(2)	110.7(2)	S(3)C(8)S(4)	110.7(2)
N(1)C(1)S(1)	124.7(3)	N(2)C(8)S(3)	125.2(3)
N(1)C(1)S(2)	123.7(3)	N(2)C(8)S(4)	124.1(3)
Angle	φ, deg	Angle	φ, deg
Au(1)S(1)S(2)C(1)	–177.8(2)	Au(2)S(3)S(4)C(8)	176.2(3)
S(1)Au(1)C(1)S(2)	–178.0(2)	S(3)Au(2)C(8)S(4)	176.6(2)
S(1)C(1)N(1)C(2)	–1.9(6)	S(3)C(8)N(2)C(9)	–179.7(4)
S(1)C(1)N(1)C(5)	179.6(3)	S(3)C(8)N(2)C(12)	–6.4(7)
S(2)C(1)N(1)C(2)	177.5(3)	S(4)C(8)N(2)C(9)	–0.28(6)
S(2)C(1)N(1)C(5)	1.0(5)	S(4)C(8)N(2)C(12)	173.0(4)
Cation C		Cation D	
Bond	*d*, Å	Bond	*d*, Å
Au(3)–S(5)	2.3348(10)	Au(4)–S(7)	2.3406(10)
Au(3)–S(6)	2.3284(11)	Au(4)–S(8)	2.3269(11)
Au(3)···S(7)[d]	3.7607(12)	Au(4)···S(5)[g]	3.5091(11)
S(5)–C(15)	1.725(4)	S(7)–C(22)	1.726(5)
S(6)–C(15)	1.736(4)	S(8)–C(22)	1.732(4)
N(3)–C(15)	1.299(5)	N(4)–C(22)	1.297(5)
N(3)–C(16)	1.476(5)	N(4)–C(23)	1.464(6)
N(3)–C(19)	1.474(5)	N(4)–C(26)	1.486(6)
Angle	ω, deg	Angle	ω, deg
S(5)Au(3)S(6)	75.55(4)	S(7)Au(4)S(8)	75.32(4)
S(5)Au(3)S(6)[c]	104.45(4)	S(7)Au(4)S(8)[f]	104.68(4)
C(15)S(5)Au(3)	86.61(13)	C(22)S(7)Au(4)	86.6(2)
C(15)S(6)Au(3)	86.57(14)	C(22)S(8)Au(4)	86.9(2)
S(5)C(15)S(6)	111.2(2)	S(7)C(22)S(8)	111.1(2)
N(3)C(15)S(5)	125.1(3)	N(4)C(22)S(7)	125.5(4)
N(3)C(15)S(6)	123.7(3)	N(4)C(22)S(8)	123.3(4)
Angle	φ, deg	Angle	φ, deg
Au(3)S(5)S(6)C(15)	178.0(2)	Au(4)S(7)S(8)C(22)	–175.7(3)
S(5)Au(3)C(15)S(6)	178.2(2)	S(7)Au(4)C(22)S(8)	–176.1(2)
S(5)C(15)N(3)C(16)	1.4(6)	S(7)C(22)N(4)C(23)	–0.9(7)
S(5)C(15)N(3)C(19)	–179.6(3)	S(7)C(22)N(4)C(26)	178.3(4)
S(6)C(15)N(3)C(16)	–178.0(3)	S(8)C(22)N(4)C(23)	180.0(4)
S(6)C(15)N(3)C(19)	0.1(6)	S(8)C(22)N(4)C(26)	–0.8(6)

Table 2. (Contd.)

Anions			
Bond	*d*, Å	Bond	*d*, Å
Fe(1)–Cl(1)	2.1891(13)	Fe(2)–Cl(5)	2.173(2)
Fe(1)–Cl(2)	2.199(2)	Fe(2)–Cl(6)	2.192(2)
Fe(1)–Cl(3)	2.1901(13)	Fe(2)–Cl(7)	2.1885(14)
Fe(1)–Cl(4)	2.1745(14)	Fe(2)–Cl(8)	2.195(2)
Angle	ω, deg	Angle	ω, deg
Cl(1)Fe(1)Cl(2)	108.49(5)	Cl(5)Fe(2)Cl(6)	108.62(7)
Cl(1)Fe(1)Cl(3)	109.67(6)	Cl(5)Fe(2)Cl(7)	109.26(7)
Cl(1)Fe(1)Cl(4)	109.09(6)	Cl(5)Fe(2)Cl(8)	112.61(7)
Cl(2)Fe(1)Cl(4)	110.25(7)	Cl(6)Fe(2)Cl(8)	108.64(6)
Cl(3)Fe(1)Cl(2)	109.09(6)	Cl(7)Fe(2)Cl(6)	108.53(6)
Cl(3)Fe(1)Cl(4)	110.22(6)	Cl(7)Fe(2)Cl(8)	109.10(6)
Compound **II**			
Cation			
Bond	*d*, Å	Bond	*d*, Å
Au(1)–S(1)	2.317(2)	S(2)–C(1)	1.713(6)
Au(1)–S(2)	2.3205(14)	N(1)–C(1)	1.313(7)
Au(1)···Cl(1)[d/e]	3.709(4)	N(1)–C(2)	1.507(10)
Au(1)···Cl(3)[b/c]	3.615(4)	N(1)–C(5)	1.475(7)
S(1)–C(1)	1.736(5)		
Angle	ω, deg	Angle	ω, deg
S(1)Au(1)S(2)	74.51(5)	C(1)S(2)Au(1)	88.3(2)
S(1)Au(1)S(2)[a]	105.49(5)	S(1)C(1)S(2)	109.0(3)
C(1)S(1)Au(1)	87.9(2)	N(1)C(1)S(1)	122.6(4)
		N(1)C(1)S(2)	128.4(4)
Angle	φ, deg	Angle	φ, deg
Au(1)S(1)S(2)C(1)	–174.1(3)	S(1)C(1)N(1)C(5)	179.2(4)
S(1)Au(1)C(1)S(2)	–174.6(2)	S(2)C(1)N(1)C(2)	179.7(5)
S(1)C(1)N(1)C(2)	–0.4(8)	S(2)C(1)N(1)C(5)	–0.7(9)
Anion			
Bond	*d*, Å	Bond	*d*, Å
Fe(1)–Cl(1)	2.161(3)	Fe(1)–Cl(3)	2.130(3)
Fe(1)–Cl(2)	2.132(4)	Fe(1)–Cl(4)	2.161(3)
Angle	ω, deg	Angle	ω, deg
Cl(1)Fe(1)Cl(2)	107.7(3)	Cl(2)Fe(1)Cl(3)	120.0(3)
Cl(1)Fe(1)Cl(3)	114.6(2)	Cl(2)Fe(1)Cl(4)	98.8(3)
Cl(1)Fe(1)Cl(4)	105.8(2)	Cl(3)Fe(1)Cl(4)	107.9(3)

* Symmetry transforms: [a] $-x+2, -y+2, -z+1$; [b] $-x+2, -y+1, -z+1$; [c] $-x+1, -y+1, -z+1$; [d] $x, -y+1\frac{1}{2}, z-1/2$; [e] $-x+1, y-1/2, -z+1\frac{1}{2}$; [f] $-x+1, -y+1, -z+2$; [g] $-x+1, y+1/2, -z+1\frac{1}{2}$; [h] $x, -y+1/2, z+1/2$ (**I**) and [a] $-x, -y+1, -z+2$; [b] $-x+1, y, -z+1\frac{1}{2}$; [c] $x-1, -y+1, z+1/2$; [d] $-x+1, -y+1, -z+1$; [e] $x-1, y, z+1$ (**II**).

The energy dispersive spectra of the latter, except for Fe, C, N, and S, show that the samples additionally contain Au and Cl (Fig. 1b'). The change in the chemical composition of the samples indicates the formation of new compounds in the systems discussed.

The unit cells of compounds **I** and **II** contain 8 and 4 formula units $[Au(S_2CNR_2)_2][FeCl_4]$ (R = C_3H_7, *iso*-C_3H_7), respectively (Fig. 2). Each compound contains centrosymmetric complex cations $[Au(S_2CNR_2)_2]^+$ and noncentrosymmetric complex tetrachloroferrate(III) ions.[1] Four structurally nonequivalent cations $[Au\{S_2CN(C_3H_7)_2\}_2]^+$ (hereinafter,

[1] It is necessary to note that the use of $[Fe(S_2CNR_2)_3]$ in the synthesis of the heteronuclear complexes did not lead to the reduction of iron(III) to iron(II) in the reaction products, the possibility of which was indicated earlier [25].

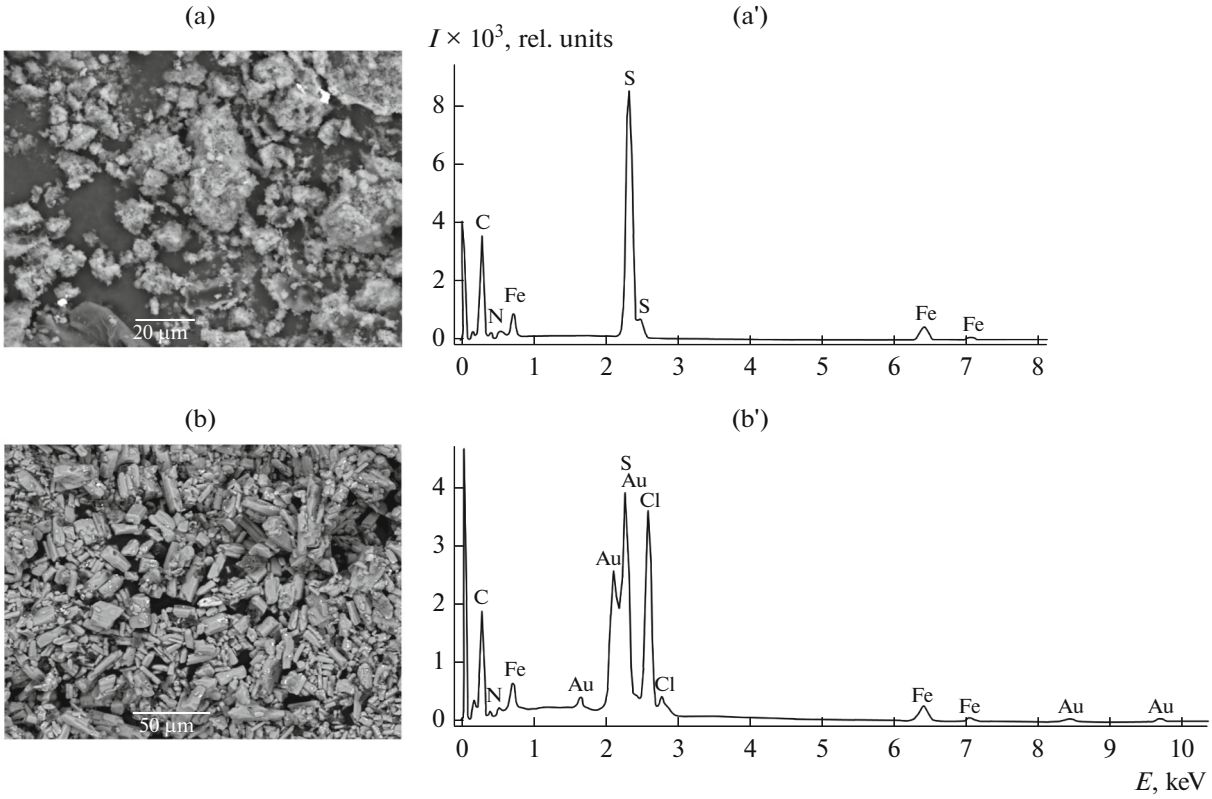

Fig. 1. (a, b) Size and shape of the particles and (a', b') the energy dispersive spectra for complexes (a, a') $[Fe\{S_2CN(C_3H_7)_2\}_3]$ and (b, b') $([Au\{S_2CN(C_3H_7)_2\}_2][FeCl_4])_n$.

cations A, B, C, and D with the Au(1), Au(2), Au(3), and Au(4) atoms, respectively) and two structurally nonequivalent anions with the Fe(1) and Fe(2) atoms are involved in the formation of the crystalline lattice of compound **I**. In compound **II**, the $[Au\{S_2CN(iso\text{-}C_3H_7)_2\}_2]^+$ cations and $[FeCl_4]^-$ anions are structurally unified.

The coordination mode close to the *S*,*S*'-isobidentate one is observed for the Dtc ligands in the complex cations of gold(III): the difference in Au–S bond lengths does not exceed 0.014 Å. The Dtc ligands in compound **II** are characterized by somewhat higher strength of binding than that for compound **I** (Table 2). The discussed coordination of the Dtc ligands by the central gold atom is accompanied by the formation of two four-membered metallocycles $[AuS_2C]$ with the common gold atom. The approached positions of the opposite atoms in the small-sized cycles $[AuS_2C]$ in compounds **I**/**II** show that the interatomic distances Au···C (2.812–2.832/2.844 Å) and S···S (2.846–2.858/2.808 Å) are substantially shorter than the sums of the van der Waals radii of the corresponding pairs of atoms: 3.36 and 3.60 Å [26–28]. In addition, the AuSSC and AuSCS torsion angles close to 180° indicate the coplanar arrangement of the atoms in the $[AuS_2C]$ groups (Table 2). Both these facts indicate a high concentration of the π-electron density and the manifestation of the *trans*-annular interaction inside the cycles. In cations B and D (**I**) and in compound **II**, the atoms discussed somewhat deviate from the plane due to the tetrahedral distortion. The geometry of the $[AuS_4]$ chromophores is close to the planar tetragonal one: the low-spin (intra-orbital) dsp^2-hybrid state of the central gold atom. The C_2NCS_2 groups of the dithiocarbamate ligands are also almost planar due to the mesomeric effect. Only the C(12) in cation B (**I**) exhibits a significant deviation from the plane (see values of the SCNC torsion angles, Table 2).

The anionic moiety of compounds **I** and **II** contains complex ions $[FeCl_4]^-$ in which the structurally nonequivalent chlorine atoms form a distorted tetrahedral environment of iron (sp^3-hybrid state). The Fe–Cl bond lengths lie in a range of 2.130–2.199 Å. The ClFeCl bond angles (98.8°–120.0°) appreciably deviate from the purely tetrahedral value. It is important that the structure of compound **I** contains two isomeric anions $[FeCl_4]^-$ with the Fe(1) and Fe(2) atoms (Fig. 3c, Table 2), whereas the $[FeCl_4]^-$ complex anion in compound **II** is disordered: each chlorine atom is statistically disordered between two structural positions with equal site occupancies (Fig. 4). The character of structural differences between the non-

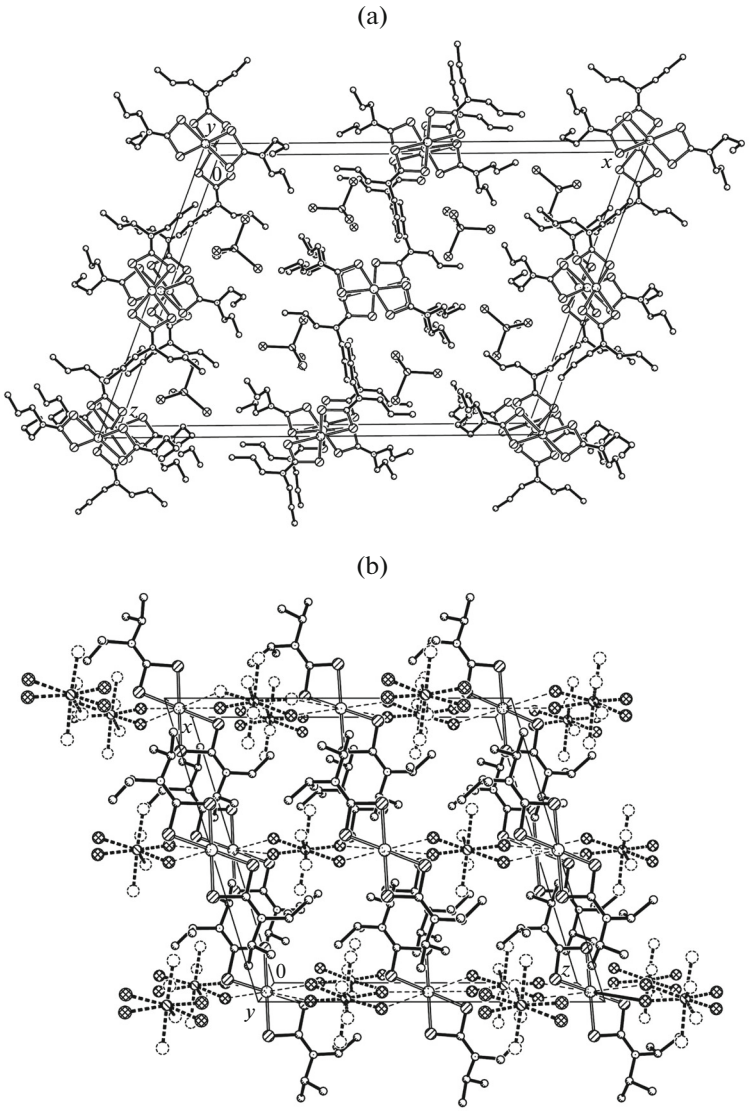

Fig. 2. Projections of the structures of compounds (a) **I** and (b) **II** on the *xz* plane.

equivalent gold(III) cations and between the iron(III) anions (Table 2) makes it possible to classify these ions as conformers.

The relatively weak Au···S (**I**) and Au···Cl (**II**) secondary interactions[2] of the nonvalent type play a determining role at the supramolecular level in the structural self-organization of the complexes. (Note that the manifestation of various secondary interactions is rather typical when constructing supramolecular structures of the gold(III) and gold(I) complexes with thio(dithio) ligands [30–35].) In the structure of compound **I**, each isomeric complex cation A, B, C, and D forms two pairs of nonsymmetric secondary bonds Au···S with the neighbors: Au(1)···S(3) and Au(1)···S(3)^{a} 3.7316, Au(2)···S(1) and Au(2)···S(1)^{b} 3.5316, Au(3)···S(7)^{d} and Au(3)···S(7)^{e} 3.7607, and Au(4)···S(5)^{g} and Au(4)···S(5)^{h} 3.5091 Å (Figs. 3a, 3b; Table 2). In cations B and D, the gold atoms form secondary Au···S bonds, whose lengths are close to the sum of the van der Waals radii of the gold and sulfur atoms: 3.46 Å [26–28]. The interactions discussed are much weaker for the gold atom in cations A and C. As a result, two independent linear cation-cationic polymeric chains $[\cdots A\cdots B\cdots]_n$ and $[\cdots C\cdots D\cdots]_n$ are formed (Figs. 3a, 3b) (oriented along the crystallographic axis *y*), and the Au(1)···Au(2) and Au(3)···Au(4) interatomic distances in them are 4.230 Å and the Au(2)Au(1)Au(2)^{a} and Au(4)^{d}Au(3)Au(4)^{e} angles are 180°. The isomeric complex anions $[FeCl_4]^-$ alternate at the right and left of the polymeric chains

[2] The concept of secondary bonds was proposed [29] for the description of interactions characterized by distances comparable with the sums of the van der Waals radii of the corresponding atoms.

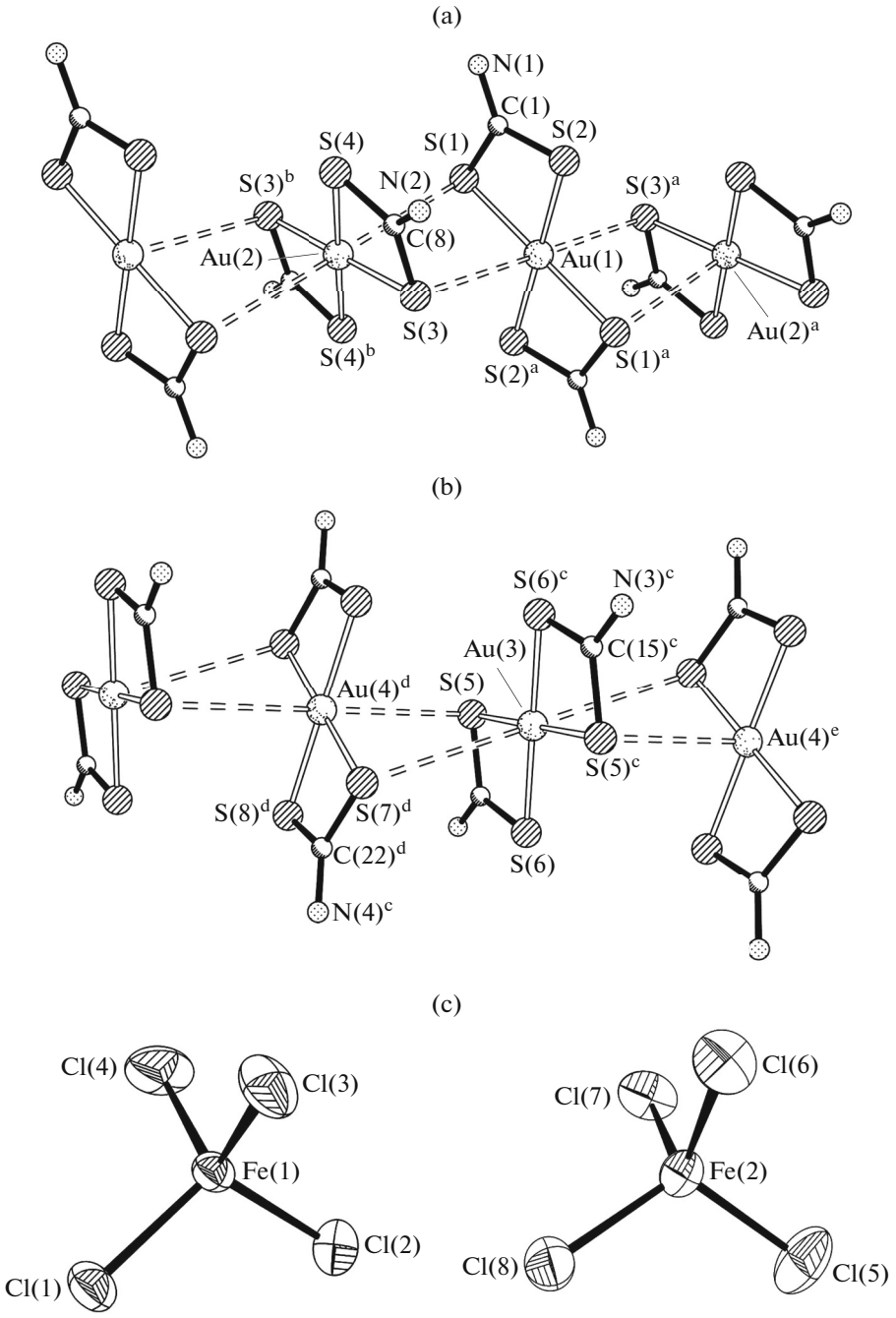

Fig. 3. (a, b) Structures of the cationic polymeric chains and (c) isomeric tetrahedral anions $[FeCl_4]^-$ in complex **I**.

(Figs. 2a, 3). The structural fragments presented in Figs. 3a and 3b show that two diagonally oriented sulfur atoms participate in the secondary interactions of each gold(III) cation. The sulfur atoms that are not involved in the secondary Au···S interactions (S(2), S(4), S(6), and S(8)) form reliably stronger intracationic covalent Au–S bonds (Table 2). The alternating isomeric cations in the polymeric chains are spatially oriented relative to each other in such a way that their bisecting planes separating the $[CS_2AuS_2C]$ bicyclic fragments form an angle of ~90° (Fig. 2a).

Compound **II** exhibits the basically different type of the supramolecular structure due to the nonvalent secondary interactions Au···Cl. Each complex cation and structurally disordered anions are involved in pair nonsymmetric secondary interactions $Au(1)\cdots Cl(1)^{d/e}$ and $Au(1)\cdots Cl(3)^{b/c}$ with the nearest neighbors to form a zigzag cation-anionic polymeric chain with the

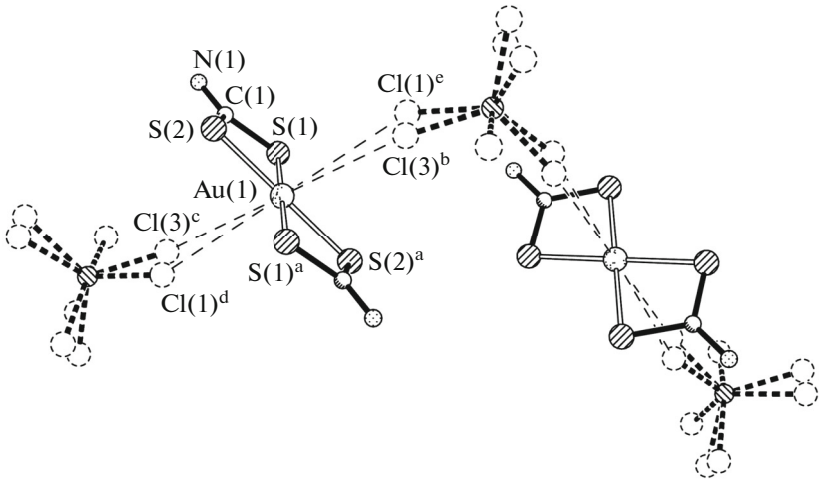

Fig. 4. Fragment of the cation-anionic polymeric chain in complex **II**.

complex cations and anions alternating along the chain length (Fig. 4). The secondary interactions involving two (Cl(1) and Cl(3)) of four chlorine atoms of the $[FeCl_4]^-$ anion are characterized by noticeably different Au···Cl distances equal to 3.709 and 3.615 Å, respectively (they exceed the sum of the van der Waals radii of gold and chlorine equal to 3.41 Å [26–28]). In the polymeric chain discussed, the Au···Fe distance is 5.671 Å and the FeAuFe and AuFeAu angles are 180° and 96.64°, respectively. The secondary interactions in the discussed cation-cationic and cation-anionic polymeric chains result in the formation by each gold atom of strongly elongated distorted octahedral chromophores $[AuS_6]$ (**I**) and $[AuS_4Cl_2]$ (**II**).

The thermal behavior of complexes **I**/**II** was studied by the STA method providing the parallel detection of the TG and DSC curves. Compound **II** containing the Dtc ligands with isostructural alkyl substituents is thermally stable at temperatures below ~130°C, which is noticeably higher than that for compound **I** (to ~110°C) containing the dipropyl dithiocarbamate ligands (Figs. 5*a*, 6*a*). The onset of the smooth mass loss is detected when the mentioned temperatures are exceeded, and the rate of the mass loss increases rapidly upon the transition to the steeply descending region of the TG curves (~175–320/~225–320°C). The main mass loss equal to 47.56/56.48% is detected at this stage, indicating that the thermolysis proceeds simultaneously at the cation and anion with the reduction of gold(III) to the metal and the liberation of $FeCl_3$. The inflection points in the TG curves in this region indicate a complicated character of the thermolysis processes. Then the TG curves reach the regions of the smooth desorption of volatile thermolysis products (mainly liberated $FeCl_3$, b.p. = 316°C [36]), and the desorption is almost completed to ~650/550°C. The residual weight at 1100°C is 32.79/36.30%, which substantially exceeds the value calculated for reduced gold (26.36%). When opening the crucibles after the completion of thermolysis, a red-brown caked mixture with inclusions of finest metallic yellow-colored balls was found on the bottom (Fig. 6*d*). The energy dispersive spectra indicate the presence of iron and oxygen in the caked slag mixture, whereas the lustrous yellow balls represent reduced metallic gold. Thus, the excessive weight of the residue should be assigned to Fe_2O_3 formed due to an oxygen impurity present in argon. According to published data [37–40], α-Fe_2O_3 was identified as the final substance of the thermolysis of various complexes containing iron(III), dithiocarbamate groups, and chloride ions (in spite of a variety of intermediate products $Fe(SCN)_3$, FeS_2, FeS, $FeSO_4$, and γ-Fe_2O_3).

For the thermolysis of compound **I** in corundum crucibles, the DSC curve in the low-temperature region detects weakly pronounced endothermic effects (Fig. 5*b*), and the DSC curves were additionally recorded in aluminum crucibles to reveal these effects more distinctly (Fig. 5*c*). In the latter case, two endothermic effects with extremes at 101.5 and 137.4°C are distinctly seen (the corresponding extrapolated temperatures are 98.0 and 130.3°C). The first endothermic effect is caused by the phase transition of the substance to a more stable modification and is not repeatedly reproduced in the programmed heating–cooling–heating regime. The second effect is attributed to the melting of the complex (a melting range of 128–130°C was established for compound **I** by the independent determination in a glass capillary).

The DSC curve of complex **II** (Fig. 6*b*) detects an endothermic effect (falls on the intensive thermolysis region), the double differentiation of which showed that this effect was a superposition of two closely arranged endothermic effects with extremes at

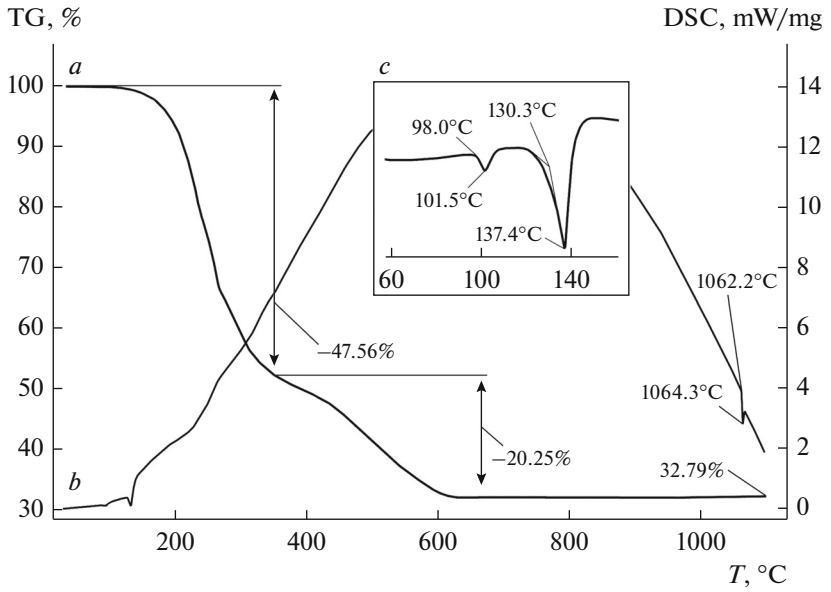

Fig. 5. (*a*) TG and (*b*) DSC curves for complex **I** with (*c*) the low-temperature region recorded in an aluminum crucible.

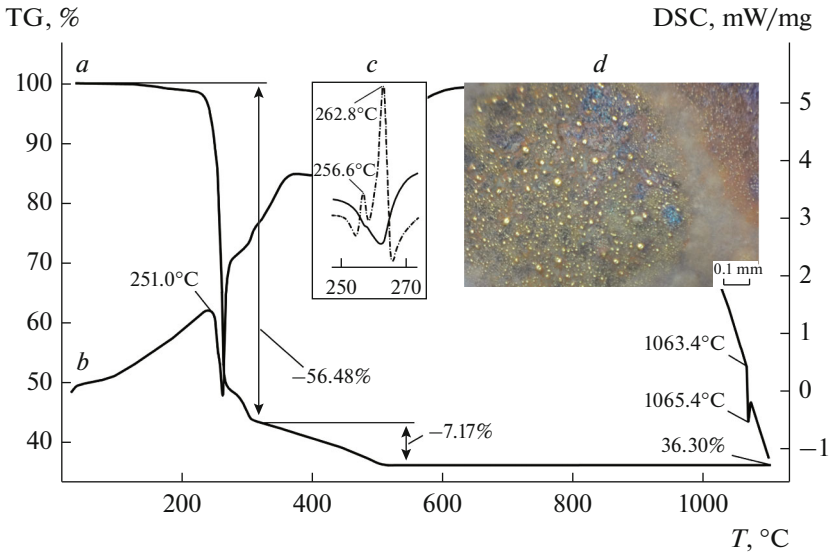

Fig. 6. (*a*) TG and (*b*) DSC curves for complex **II**, (*c*) the second derivative of the endothermic effect caused by melting followed by the thermal destruction of the substance (shown by dashed line), and (*d*) slag particles with metallic gold balls after the completion of thermolysis.

256.6 and 262.8°C (Fig. 6*c*). The former is due to the melting of the sample (the extrapolated m.p. is 251.0°C), and the latter is caused by the thermolysis of the complex. The melting of the sample was established independently (in a glass capillary) at 250–252°C (with the transition to destruction accompanying by gas release). The endothermic effects in the high-temperature region (Figs. 5*b*, 6*b*) are attributed to the melting of the reduced gold particles: the extrapolated m.p. are 1062.2/1063.4°C.

ACKNOWLEDGMENTS

The studies were carried out at the Far East Center for X-ray Structural Investigations and the Analytical Center at the Institute of Geology and Nature Management of the Far East Branch of the Russian Academy of Sciences (electron scanning microscopy and X-ray spectral microanalysis).

This work was supported in part by the Presidium of the Far East Branch of the Russian Academy of Sciences (program "Far East," project no. 15–I–3–001)

and the Ministry of Education and Science of the Russian Federation (project no. 1452.2014/9).

REFERENCES

1. Coucouvanis, D., *Prog. Inorg. Chem.*, 1979, vol. 26, p. 301.
2. Golding, R.M., Tennant, W.C., Kanekar, C.R., et al., *J. Chem. Phys.*, 1966, vol. 45, no. 7, p. 2688.
3. Eley, R.R., Duffy, N.V., and Uhrich, D.L., *J. Inorg. Nucl. Chem.*, 1972, vol. 34, no. 12, p. 3681.
4. Chapps, G.E., McCann, S.W., Wickman, H.H., and Sherwood, R.C., *J. Chem. Phys.*, 1974, vol. 60, no. 3, p. 990.
5. Law, N.A., Dietzsch, W., and Duffy, N.V., *Polyhedron*, 2003, vol. 22, no. 27, p. 3423.
6. Grekova, A.V., Ivanchenko, P.A., and Seifullina, I.I., *Vopr. Khim. Khim. Tekhnol.*, 2012, no. 1, p. 42.
7. Yoshimura, T. and Kotake, A., *Antioxid. Redox Signal.*, 2004, vol. 6, no. 3, p. 639.
8. Vanin, A.F., Bevers, L.M., Mikoyan, V.D., et al., *Nitric Oxide*, 2007, vol. 16, no. 1, p. 71.
9. Vanin, A.F., Poltorakov, A.P., Mikoyan, V.D., et al., *Nitric Oxide*, 2006, vol. 15, no. 4, p. 295.
10. Rodina, T.A., Ivanov, A.V., Gerasimenko, A.V., et al., *Polyhedron*, 2012, vol. 40, no. 1, p. 53.
11. Ivanov, A.V., Rodina, T.A., and Loseva, O.V., *Russ. J. Coord. Chem.*, 2014, vol. 40, no. 12, p. 875.
12. Loseva, O.V. and Ivanov, A.V., *Russ. J. Inorg. Chem.*, 2014, vol. 59, no. 12, p. 491.
13. Loseva, O.V., Rodina, T.A., and Ivanov, A.V., *Russ. J. Coord. Chem.*, 2013, vol. 39, no. 6, p. 463.
14. Loseva, O.V., Rodina, T.A., Smolentsev, A.I., and Ivanov, A.V., *J. Struct. Chem.*, 2014, vol. 55, no. 5, p. 901.
15. Ivanov, A.V., Sergienko, V.I., Gerasimenko, A.V., et al., *Russ. J. Coord. Chem.*, 2010, vol. 36, no. 5, p.353.
16. Rodina, T.A., Loseva, O.V., Smolentsev, A.I., and Ivanov, A.V., *J. Struct. Chem.*, 2016, vol. 57, no. 1, p. 146.
17. Zaeva, A.S., Ivanov, A.V., Gerasimenko, A.V., and Sergienko, V.I., *Russ. J. Inorg. Chem.*, 2015, vol. 60, no. 2, p. 203.
18. Zaeva, A.S., Ivanov, A.V., and Gerasimenko, A.V., *Russ. J. Coord. Chem.*, 2015, vol. 41, no. 10, p. 644.
19. Ivanov, A.V., Bredyuk, O.A., Loseva, O.V., and Rodina, T.A., *Russ. J. Coord. Chem.*, 2015, vol. 41, no. 2, p. 108.
20. Ivanov, A.V., Bredyuk, O.A., Loseva, O.V., and Antzutkin, O.N., *Russ. J. Inorg. Chem.*, 2016, vol. 61, no. 6, p. 755.
21. Ivanov, A.V., Loseva, O.V., Rodina, T.A., et al., *Russ. J. Coord. Chem.*, 2016, vol. 42, no. 2, p. 104.
22. Byr'ko, V.M., *Ditiokarbamaty* (Dithiocarbamates), Moscow: Nauka, 1984.
23. *APEX2*, Madison: Bruker AXS, 2010.
24. Sheldrick, G.M., *Acta Crystallogr., Sect. A: Found. Adv.*, 2015, vol. 71, no. 1, p. 3.
25. Exarchos, G., Robinson, S.D., and Steed, J.W., *Polyhedron*, 2001, vol. 20, nos. 24–25, p. 2951.
26. Pauling, L., *The Nature of the Chemical Bond and the Structure of Molecules and Crystals*, London: Cornell Univ., 1960.
27. Bondi, A., *J. Phys. Chem.*, 1964, vol. 68, no. 3, p. 441.
28. Bondi, A., *J. Phys. Chem.*, 1966, vol. 70, no. 9, p. 3006.
29. Alcock, N.W., *Adv. Inorg. Chem. Radiochem.*, 1972, vol. 15, no. 1, p. 1.
30. Olmos, M.E., *Modern Supramolecular Gold Chemistry: Gold-Metal Interactions and Applications*, Laguna, A., Ed., Weinheim: Wiley, 2008, p. 295.
31. Castiñeiras, A., Dehnen, S., Fuchs, A., et al., *Dalton Trans.*, 2009, no. 15, p. 2731.
32. Han, S., Jung, O.-S., and Lee, Y.-A., *Transition Met. Chem.*, 2011, vol. 36, no. 7, p. 691.
33. Koskinen, L., Jääskeläinen, S., Kalenius, E., et al., *Cryst. Growth Des.*, 2014, vol. 14, no. 4, p. 1989.
34. Khan, E., Khan, U.A., Badshah, A., et al., *J. Mol. Struct.*, 2014, vol. 1060, p. 150.
35. Rodina, T.A., Korneeva, E.V., Antzutkin, O.N., and Ivanov, A.V., *Spectrochim. Acta, Part A,* 2015, vol. 149, p. 881.
36. Lidin, R.A., Andreeva, L.L., and Molochko, V.A., *Spravochnik po neorganicheskoi khimii* (Handbook in Inorganic Chemistry), Moscow: Khimiya, 1987.
37. Kaushik, N.K., Chattwal, G.R., and Sharma, A.K., *J. Therm. Anal.*, 1983, vol. 26, no. 2, p. 309.
38. Singhal, S., Sharma, C.L., Garg, A.N., and Chandra, K., *Transition Met. Chem.*, 2001, vol. 26, nos. 1–2, p. 81.
39. Singhal, S., Garg, A.N., and Chandra, K., *J. Alloys Compd.*, 2007, vol. 428, nos. 1–2, p. 72.
40. Pastorek, R., Šarha, P., Peterek, T., and Trávníček, Z., *Polyhedron*, 2011, vol. 30, no. 17, p. 2795.

Translated by E. Yablonskaya